Clean Technologies and Recycling

Clean Technologies and Recycling, 6 (2): 122–138.
DOI: 10.3934/ctr.2026006
Received: 04 August 2025
Revised: 02 February 2026
Accepted: 12 February 2026
Published: 20 March 2026

https://www.aimspress.com/journal/ctr

Research article

Spectral IR reflectance analysis of black polymer samples with different electrical conductivities. Important results concerning plastics recycling

Wolfgang Becker*, Wenka Schweikert, Stephan Müller and Patrick Weiss

Fraunhofer Institute for Chemical Technology, Joseph-von-Fraunhoferstrasse 7, 76327 Pfinztal, Germany

***Correspondence:** Email: Wolfgang.Becker@ict.fraunhofer.de.

Abstract: The infrared spectroscopic analysis of black polypropylene (PP) polymers with varying electrical conductivities shows that increasing conductivity leads to a pronounced attenuation or complete masking of characteristic infrared absorption bands. This behavior arises from interactions between the incident electromagnetic radiation and free charge carriers, thereby limiting the applicability of Fourier-transform infrared (FTIR) spectroscopy for reliable material identification. Comparable limitations may also occur in non-black polymers that exhibit sufficiently high electrical conductivity. Theoretical modeling and experimental measurements of the samples are presented.

Keywords: plastic recycling; electrically conductive polymer samples; black plastic samples; theoretical description; comparison of theory and measured spectra

1. Introduction

1.1. Materials and technologies in plastic recycling

The worldwide production and consumption of plastics has been increasing continuously over the past decades, leading to a steadily growing amount of plastic waste, which has become a major environmental and economic challenge [1,2]. As a consequence, efficient recycling strategies have become essential to reduce environmental pollution, conserve resources, and support the circular economic concept. A key prerequisite for high-quality plastic recycling is the reliable sorting and identification of polymer materials, as even small fractions of misclassified plastics can significantly deteriorate the properties of recycled products.

With increasing material diversity and the widespread use of additives, fillers, and functional modifiers, the requirements for accurate polymer classification have become progressively more complex. Modern recycling streams contain a broad spectrum of materials ranging from commodity plastics to highly engineered technical polymers, often combined with pigments, reinforcements, or electrically functional components. Consequently, simple physical separation techniques are no longer sufficient, and a variety of analytical and spectroscopic measurement methods are employed to enable reliable material identification and quality assessment [3]. These include, among others, near-infrared (NIR) spectroscopy, mid-infrared (MIR) spectroscopy, Raman spectroscopy, laser-induced breakdown spectroscopy (LIBS), and X-ray-based techniques, each with specific advantages and limitations [4–9].

Among these methods, spectroscopic techniques play a central role due to their non-destructive nature and potential for automated, high-throughput operation. In industrial sorting applications, NIR spectroscopy is currently the most widely used approach, owing to its robustness and high measurement speed. However, NIR spectroscopy exhibits a fundamental limitation when applied to dark or black plastics, as carbon-based pigments strongly absorb the incident radiation, resulting in negligible reflected signals.

Mid-infrared or Fourier-transform infrared (FTIR) spectroscopy has therefore been proposed as an alternative for the identification of black plastics, as it probes fundamental molecular vibrations that are, in principle, independent of color [10]. In industrial plastic recycling, NIR spectroscopy is the dominating technique in sorting lines for polymer identification. However, NIR spectroscopy fails for dark and black plastics due to strong absorption by carbon-based pigments, which has motivated the consideration of mid-infrared (FTIR) spectroscopy as a potential alternative. While FTIR can, in principle, enable the identification of black polymers, increasing electrical conductivity leads to a suppression of characteristic infrared spectral features, resulting in misclassification and directly affecting the quality of recycled material streams. For many black polymer materials with zero or low electrical conductivity, characteristic infrared reflectance features remain clearly detectable (Figure 1). No differences can be detected between the spectrum of the transparent (non-black) sample and that of the black sample. Both samples have been measured with an FTIR spectrometer system with the same spectral resolution of 4 cm^{-1} with a reflection probe.

Nevertheless, modern plastic formulations increasingly incorporate conductive additives such as carbon black, graphite, or carbon nanotubes to achieve antistatic or electrically conductive properties. As a result, a growing fraction of black plastics encountered in recycling streams exhibits significant electrical conductivity.

From a physical standpoint, increasing electrical conductivity introduces free charge carriers that strongly interact with electromagnetic radiation. This interaction modifies the dielectric response of the material and can suppress or mask vibrational absorption features in the infrared spectral range. Despite its practical relevance for plastic recycling, the influence of electrical conductivity on infrared reflectance spectra and thus on the applicability of FTIR spectroscopy for polymer identification has not yet been systematically investigated.

The present work addresses this gap by analyzing the infrared reflectance behavior of black polypropylene (PP) composites with systematically varied electrical conductivities. Experimental FTIR reflectance measurements are combined with a physically motivated theoretical description based on a Lorentz–Drude model to elucidate the transition from vibration-dominated to free-carrier-

dominated optical response. The results provide a quantitative understanding of the conductivity range in which FTIR-based material identification becomes unreliable, thereby offering valuable guidance for the selection and limitation of spectroscopic methods in plastic recycling applications.

In industrial plastic recycling, reliable material identification is further complicated by the strong heterogeneity of real waste streams. Incoming materials are often contaminated by dirt, organic residues, coatings, or multilayer structures, all of which can distort or obscure material-specific spectral signatures. In addition, plastics typically contain a wide range of additives and fillers such as plasticizers, flame retardants, glass fibers, black carbon, or mineral fillers that alter optical properties and may lead to misclassification. The key novelty of this work is the demonstration that the loss of IR spectral features in black polymers is governed by electrical conductivity rather than color alone.

These factors affect infrared methods and limit the reproducibility and interpretability of infrared (IR) reflectance spectra. However, such general measurement-related challenges are not the primary focus of the present work and are mentioned here solely to provide context for the more specific conductivity-related effects discussed below.

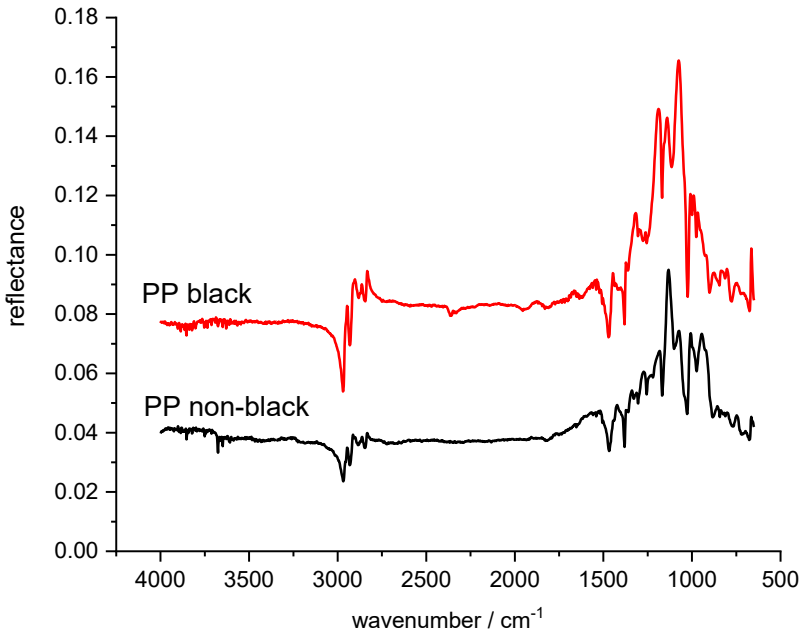

Figure 1. Comparison of the reflectance spectra of non-black and black polypropylene (PP) samples with zero electrical conductivity. Distinct characteristic reflectance peaks are observed in both samples, independent of polymer color. The black coloration of the PP sample was achieved by the addition of a black masterbatch with no electrical conductivity.

1.2. Theoretical description

In the following section, we introduce a theoretical description of the optical behavior of plastics to distinguish material-specific spectral effects from measurement-related artifacts and to achieve a physically grounded interpretation of the observed reflectance behavior. Such a model allows the

influence of free charge carriers and molecular vibrational modes to be treated separately and provides insight into the mechanisms responsible for the attenuation of infrared features. Moreover, a theoretical framework enables the results obtained for polypropylene to be transferred to other polymer systems exhibiting electrical conductivity, thereby extending the relevance of the present study beyond the specific material investigated here.

The optical behavior of materials can fundamentally be described by their dielectric function. This function characterizes how a material interacts with electromagnetic radiation and provides information on absorption, reflection, and transmission as a function of frequency. In the case of solid materials, especially polymers, the dielectric function consists of several contributions that can be effectively modeled.

A well-established approach for describing the optical properties of solid polymers is based on oscillator models. These models allow for a physically grounded simulation of spectra by representing the material response as a superposition of individual resonant oscillations. The dominant contributions in the infrared and visible spectral range stem from bound charges, such as vibrations of functional groups, which are mathematically described by the Lorentz oscillator model [11–13]. This model captures the spectral response of such bound charge carriers and allows for a realistic reproduction of the characteristic absorption bands. The spectral shape is governed by three fundamental parameters: the eigenfrequency of the oscillation (resonance frequency), the oscillator strength (intensity of the contribution), and the damping factor (width of the resonance).

When a polymer exhibits electrical conductivity, free charge carriers—primarily electrons—appear in addition to the bound vibrational modes. These free electrons significantly affect the dielectric function and lead to additional optical phenomena, such as increased infrared reflectivity or suppression of vibrational absorption bands. Their influence is effectively described by the Drude model, which captures the motion of free carriers under electromagnetic fields and includes scattering processes characterized by a relaxation time. It specifically explains enhanced reflectivity at low frequencies (e.g., THz or IR) and the suppression or overlapping of characteristic absorption bands in highly conductive materials.

By combining the Lorentz and Drude models, the complete spectral behavior of a conductive polymer can be comprehensively described. While the Lorentz component accounts for resonant vibrations of bound charges, the Drude component models the response of free electrons.

In the classical Drude model, a constant relaxation time τ is assumed. This approximation is valid, for instance, in ideal, single-crystalline metals without lattice defects or grain boundaries. At a low temperature, phonon populations are significantly reduced, which limits scattering processes for charge carriers such as electrons. Under such conditions, the Drude model with a constant τ provides an adequate description.

In real materials, however, various types of disorders are present, including structural defects, grain boundaries, impurities, and nanostructures. At elevated temperatures, additional phonon excitations enhance electron–phonon scattering, making the relaxation time τ temperature-dependent. This temperature dependence will not be further addressed in the present work.

The polypropylene (PP) samples investigated here consist not only of the amorphous polymer matrix but also include nanoscale carbon nanotubes (CNT) and graphite powder. This complexity results in a higher density of different scattering centers within the material. Since electron scattering

at different centers depends on electron energy, the scattering behavior becomes frequency-dependent, and consequently, the relaxation time also varies with frequency, τ = τ(ν) [14]. Incorporating this into the dielectric response leads to the extended Drude model [15, 16]:

$$\tilde{\varepsilon}(\upsilon) = \varepsilon_\infty - \frac{\sigma_{DC}}{2\pi\varepsilon_0 c\,\upsilon\left(1 + i\,2\pi\,c\,\upsilon\,\tau(\upsilon)\right)} + \sum_j \frac{S_j\ \upsilon_{0,j}^2}{\upsilon_{0,j}^2 - \upsilon^2 - i\,\gamma_j\,\upsilon} \qquad (1)$$

$\tilde{\varepsilon}(\upsilon)$: complex dielectric function as a function of the wavenumber υ.
ε_∞: high-frequency dielectric constant.
ε_0: dielectric constant.

Drude term (first term):
σ_{DC}: electrical conductivity S/cm.
$\tau(\upsilon)$: frequency dependent relaxation time in seconds.
c: speed of light cm/s.

Lorentz oscillator(s) (summation term):
S_j: Oscillator strength of the respective Lorentz oscillator.
$\upsilon_{0,j}$: Resonance wavenumber cm^{-1}.
γ_j: Linewidth or damping constant cm^{-1}.

To model the observed frequency-dependent scattering behavior, the relaxation time τ(ν) was assumed to follow the empirical form shown in Eq. (2):

$$\tau(\upsilon) = \frac{\tau_0}{(1+\frac{\upsilon}{\upsilon_c})^n} \qquad (2)$$

τ(ν): frequency-dependent relaxation time in seconds of the free charge carriers.
τ_0: relaxation time in seconds in the low-frequency limit (ν→0).
ν_c: ("collision frequency" or "characteristic frequency"): the frequency in seconds at which the relaxation time has dropped to approximately half of τ_0.
n: exponential decay factor that determines how strongly τ(ν) decreases with increasing frequency.

This expression ensures the correct limiting behavior for both low and high frequencies and reflects the physical expectation that scattering processes become more effective at higher excitation frequencies. The functional form is inspired by the extended Drude model formalism and provides sufficient flexibility to fit experimental reflectance spectra. Although not directly derived from a microscopic theory, it represents a phenomenological approach commonly used in the optical modeling of disordered and nanostructured materials.

The dielectric function can be written in a real part $\varepsilon_1(\upsilon)$ and a complex part $\varepsilon_2(\upsilon)$:

$$\tilde{\varepsilon}(\upsilon) = \varepsilon_1(\upsilon) + i\varepsilon_2(\upsilon) \qquad (3)$$

The complex dielectric function $\tilde{\varepsilon}(\upsilon)$ is related to the complex refractive index $\tilde{n}(\upsilon) = n(\upsilon) + i\kappa(\upsilon)$ via the Maxwell relation as follows:

$$\tilde{n}^2 = \tilde{\varepsilon}(\upsilon) = \varepsilon_1(\upsilon) + i\varepsilon_2(\upsilon) \tag{4}$$

$$n(\upsilon) = \sqrt{\frac{\sqrt{\varepsilon_1^2(\upsilon)+\varepsilon_2^2(\upsilon)} + \varepsilon_1(\upsilon)}{2}} \tag{5}$$

$$\kappa(\upsilon) = \sqrt{\frac{\sqrt{\varepsilon_1^2(\upsilon)+\varepsilon_2^2(\upsilon)} - \varepsilon_1(\upsilon)}{2}} \tag{6}$$

$n(\upsilon)$ is the real part of the refractive, and $\kappa(\upsilon)$ is the imaginary part of the refractive index $\tilde{n}$.

This leads to the following expression for the reflectance $R(\upsilon)$ at normal incidence:

$$R(\upsilon) = \frac{(n(\upsilon) - 1)^2 + \kappa(\upsilon)^2}{(n(\upsilon) + 1)^2 + \kappa(\upsilon)^2} \tag{7}$$

1.3. Simulated IR spectra

Figure 2 shows synthetically calculated reflectance spectra of a model material in the mid-infrared range. The calculations are based on the dielectric function according to Eq. (1) and the corresponding reflectance derived from Eq. (7) using the Lorentz–Drude formalism. The representation is not intended to reproduce the exact infrared spectrum of real plastics (such as polypropylene) but rather to illustrate the influence of the specific electrical conductivity σ on the spectral reflectance behavior. To ensure comparability across all simulations and to isolate the effect of electrical conductivity on reflectance, all other model parameters were kept constant. Specifically, the relaxation time of the free carriers was set to $\tau_0=10^{-14}$ s, the damping constant of the Lorentz oscillators to ν_c =1500 [cm^{-1}], and the high-frequency dielectric constant to ε_∞=3.

In the leftmost diagram (σ = 0 S/cm), four distinct reflectance bands are visible around 2900, 2800, 1500, and 800 cm^{-1}. These bands result from Lorentz oscillators modeling characteristic IR-active vibrational modes. At low conductivity, the reflectance spectrum exhibits pronounced modulation with clearly defined minima and maxima—typical for a material dominated by bound charge excitations.

In the second diagram (σ = 1 S/cm), the influence of electrical conductivity is already clearly noticeable. Compared to σ = 0 S/cm, the spectral features appear significantly attenuated, indicating that even a small contribution of free charge carriers leads to damping of the Lorentz resonances.

As conductivity increases further—as shown in the diagrams for σ = 10 S/cm (center right) and σ = 100 S/cm (right)—the Lorentzian oscillations become progressively suppressed. The reflectance curve flattens, and the spectral fine structure nearly vanishes. In these regimes, the optical response is

increasingly dominated by the Drude contribution of the free carriers.

Overall, the simulations in Figure 2 clearly demonstrate how increasing specific electrical conductivity σ causes a transition from dielectric-like to more metallic-like reflectance behavior. The spectral features associated with bound vibrational modes are gradually masked by the growing influence of free charge carriers.

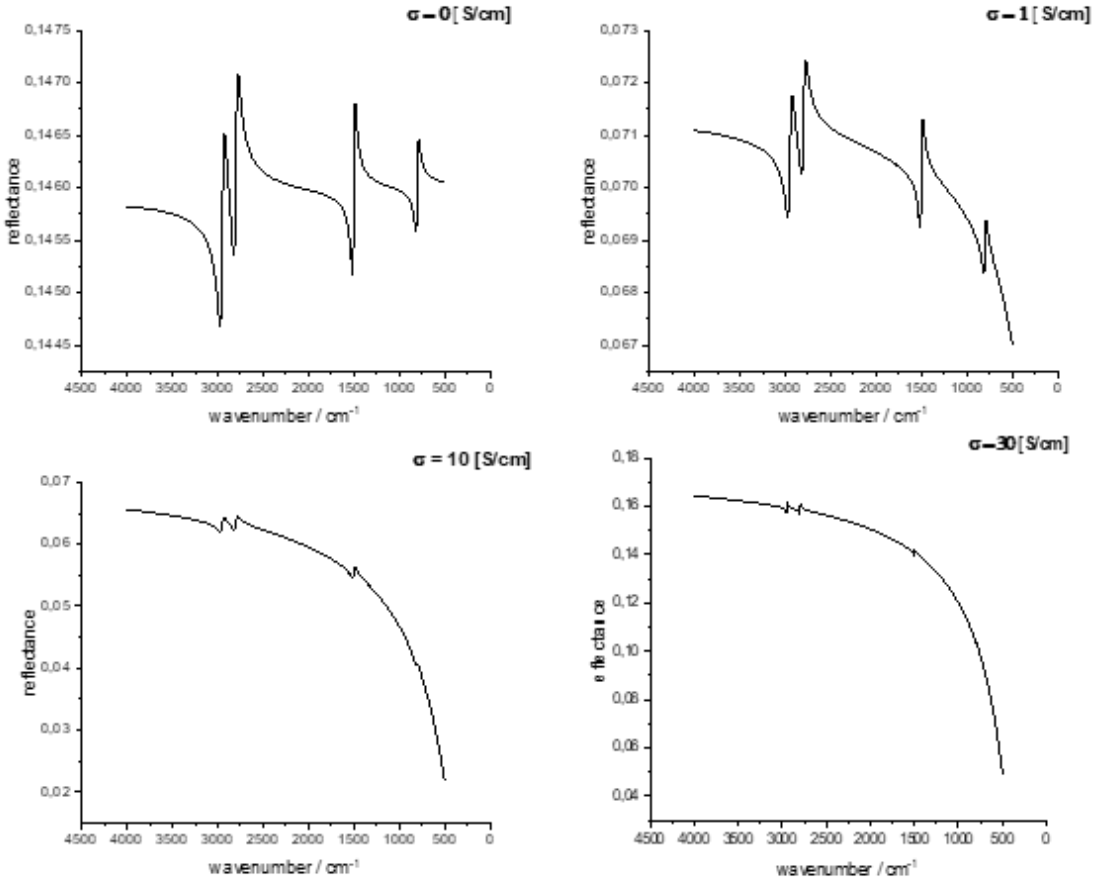

Figure 2. Spectral reflectance obtained from four simulations with different electrical conductivities σ. With increased conductivity, a pronounced reduction of spectral features is observed, which can be attributed to the increasing dominance of free charge carriers. The resonances (Lorentz oscillators) are increasingly subdued. At lower wavenumbers, the reflectance curve exhibits a negative curvature toward lower reflectance values.

2. Materials and methods

2.1. Sample preparation

Commercial polypropylene (PP) plastic was used for the samples, which were produced by extrusion, injection molding, or pressing. No specific pretreatment, such as cleaning or drying, was applied. The PP was supplied in granular form, allowing it to be processed in controlled quantities. PP

granulate was used as the base material for sample preparation. The PP was compounded with carbon nanotubes (CNTs) and graphite. CNTs were incorporated to impart electrical conductivity to the composite, while graphite served to improve the dispersion of the conductive fillers within the polymer matrix and to facilitate processability during extrusion. Moreover, graphite is assumed to support the formation of conductive pathways by occupying interstitial spaces between CNTs, thereby enhancing the percolation behavior. The CNT content varied between 1 wt% and 3 wt%, whereas the graphite content ranged from 50 wt% to 57 wt%. The CNT and graphite contents refer to nominal compositions defined during compounding; no independent post-processing quantification was performed.

The screw geometry, extrusion speed, melt temperature, and die temperature were chosen to achieve optimal mixing of the components. This allowed the production of samples with specifically adjusted electrical conductivities. After extrusion, the composite material was re-granulated and subsequently processed into plates.

Before incorporating CNTs into a polymer matrix to achieve electrical conductivity, it is essential to ensure that the CNTs themselves are conductive. In this context, a distinction must be made between single-walled carbon nanotubes (SWCNTs) and multi-walled carbon nanotubes (MWCNTs), as they can differ significantly in their properties, particularly in terms of charge transport. A key factor influencing the electrical conductivity of CNTs is their chirality, i.e., the specific way in which the graphene sheet is rolled into a tube [17].

When CNTs and graphite are embedded into the polymer, the extrusion process must be carefully controlled to ensure that a sufficient amount of CNTs and graphite leads to the formation of a percolation network. This means that the CNTs must come into contact with each other to form continuous, electrically conductive pathways throughout the polymer sample [18,19].

A further requirement for the extrusion process is that, once the percolation threshold is reached, the conductive structure within the polymer must not be disrupted by mechanical forces acting during processing. Therefore, the process must be highly controlled and reproducible.

To ensure the quality and consistency of the composite material, the use of an inline sensor for monitoring electrical conductivity during the manufacturing process is recommended [20]. Morphological aspects such as filler dispersion and surface microstructure were not systematically analyzed in this study, as the primary focus was on the optical response as a function of electrical conductivity.

A quantitative determination of the CNT and graphite contents by infrared spectroscopy is not feasible for the investigated samples. Due to the high electrical conductivity of the composites, free charge carriers dominate the optical response, leading to strong reflection and limited penetration depth of the infrared radiation. As a result, characteristic vibrational features of the additives and the polymer matrix are significantly suppressed or fully masked, preventing reliable quantitative analysis by FTIR methods.

2.2. Measurement of specific electrical conductivity of polymer plates

To determine the electrical conductivity, a four-point probe measurement was carried out using a Keithley 2400 system. Four electrodes were linearly positioned on the surface of the plastic sample (Figure 3). A constant current was applied through the outer electrodes (x_1 and x_4), while the voltage drop was measured across the inner electrodes (x_2 and x_3). This arrangement effectively eliminates the

influence of contact resistance, which is particularly crucial for materials with low conductivity, such as plastics. The electrical conductivity σ is calculated from the measured voltage drop *U*, the applied current *I*, and the sample geometry, with s = x3−x2 being the distance between the voltage probes and A = b·d the cross-sectional area (with *d* the sample thickness and *b* its width), according to the relation:

$$\sigma = \frac{I}{U}\frac{s}{A}$$

This equation for determining and measuring the electrical conductivity σ is valid for infinitely large samples or samples with large geometric dimensions, where the current flow is not disturbed. However, in realistic samples with finite geometries, the measurements are influenced and thus distorted. Therefore, the measurements must be corrected using a correction function F(d,s), and the equation for calculating σ becomes:

$$\sigma = \frac{1}{F(d,s)}\frac{I}{U}\frac{s}{A}$$

The correction functions are either tabulated or available analytically for simple geometries. They distinguish between thick and thin sample geometries. More details are found in [21,22].

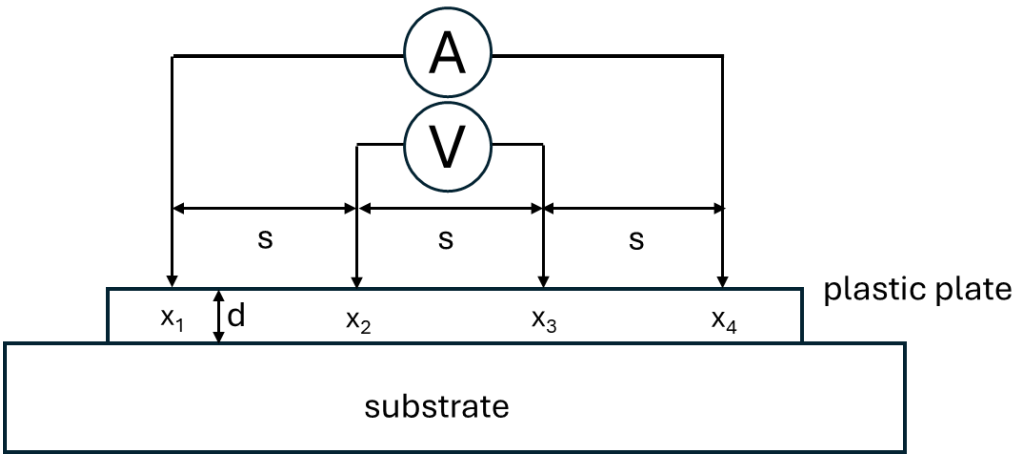

Figure 3. Schematic diagram of the four-point probe setup for measuring the specific electrical conductivity.

In Figure 4, a plastic plate is shown, on which electrical conductivity measurements were performed. The four-point probe (FPP) used for the measurements can be seen in the upper right corner of the image. Several measurements were taken at different positions on the sample. The FPP was gently pressed onto the surface of the sample. A measurement value was recorded only when a stable reading was achieved. The measurements were then evaluated according to the equations for the specific conductivity provided above.

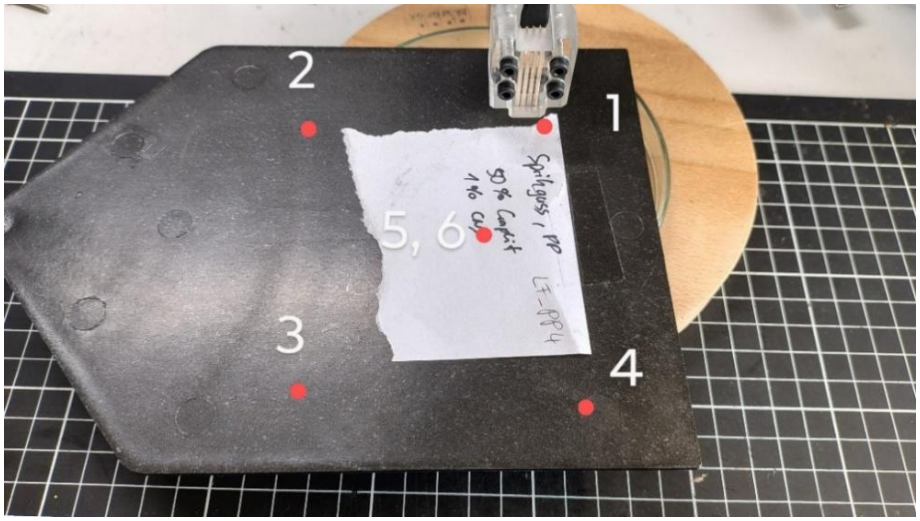

Figure 4. Illustration and image of an electrical conductivity measurement on a plastic plate. The four-point probe is visible in the upper right corner. Up to six measurements were taken at different positions on the sample.

Table 1. Sample compositions, processing methods, surface treatments, and average values of the specific electrical conductivity. The average values were calculated based on six measurements taken at different locations on each sample (see Figure 4). An exception is sample LF PP1, for which seven measurements were taken on the sample surface.

Sample name	Mixture	Fabrication process	Sample surface	Specific conductivity* (S/cm)
LF PP1	CNT 3% Graphite 57%	Hot pressing	Ground	24 (average from 7 measurements at different points)
LF PP2	CNT 3% Graphite 57%	Extrusion	No pretreatment	2.4 (average from 6 measurements at different points)
LF PP3	CNT 1% Graphite 50%	Extrusion	No pretreatment	5.3 (average from 6 measurements at different points)
LF PP4	CNT 1% Graphite 50%	Injection molding	No pretreatment	0.019 (average from 6 measurements at different points)
LF PP5	CNS 10%	Extrusion	No pretreatment	4.6 (average from 6 measurements at different points

The samples were not pretreated, i.e., no additional cleaning or surface treatment was carried out in order to avoid altering the measurement results. However, care was taken to place the probe only on

areas of the sample free from visible surface layers or moisture, as these could have significantly distorted the measurements. The locations of the six measurement points on the sample surface are shown in Figure 4. Table 1 shows the sample compositions, processing methods, surface treatments, and average values of the specific electrical conductivity. The average values were calculated based on six measurements taken at different locations on each sample (see Figure 4). An exception is sample LF PP1, for which seven measurements were taken on the sample surface. shows the samples along with their composition, manufacturing process, surface treatment, and the results of the electrical conductivity measurements

3. Results and discussion

Infrared spectroscopy of polymer samples poses several practical challenges. In particular, the condition of the sample surface plays a crucial role in the quality of the measurements. Contaminants, surface residues, moisture films, or mechanical damage, such as scratches, can significantly influence the recorded reflectance spectrum. Such effects often lead to the overlay or distortion of the actual material-specific signals. A scratched surface, for example, increases diffuse reflection, which not only reduces signal intensity but can also alter the position and shape of absorption bands. As a result, misinterpretations are likely, especially in automated analysis workflows.

Despite careful sample preparation and selection of suitable measurement points, some of the samples examined in this study exhibited surface imperfections that could not be fully avoided. In the following section, the measured reflectance spectra of all five samples are compared with their respective simulated curves. Each sample is discussed individually, with a focus on the degree of spectral structure, the reflectance behavior at low wavenumbers, and any discrepancies between measured and fitted conductivity values. Surface-related artifacts and uncertainties are explicitly considered in the interpretation. The values of all fitting parameters are given in Table 2. Measured and modeled spectra are shown in Figure 5.

Table 2. Results of the fit parameters from fitting the fit function Eq. (1) to the measured spectra. Column 3 contains the measured values of the specific conductivities, and column 2 contains the values from the fitting process.

Sample	σ_{Fit} S/cm	σ_{mess} S/cm	τ s	ν_C cm^{-1}	n	ε_∞
LF PP1	26	24	$1 \cdot 10^{-14}$	1000	1	6
LF PP2	5	2.7	$3 \cdot 10^{-14}$	650	1	6
LF PP3	/	5.3	/	/	/	/
LF PP4	6.5	0.019	$1 \cdot 10^{-14}$	1200	1	5
LF PP5	7	4.6	$4 \cdot 10^{-14}$	1000	1	6.5
PP black	0	0	/	/	/	2.8

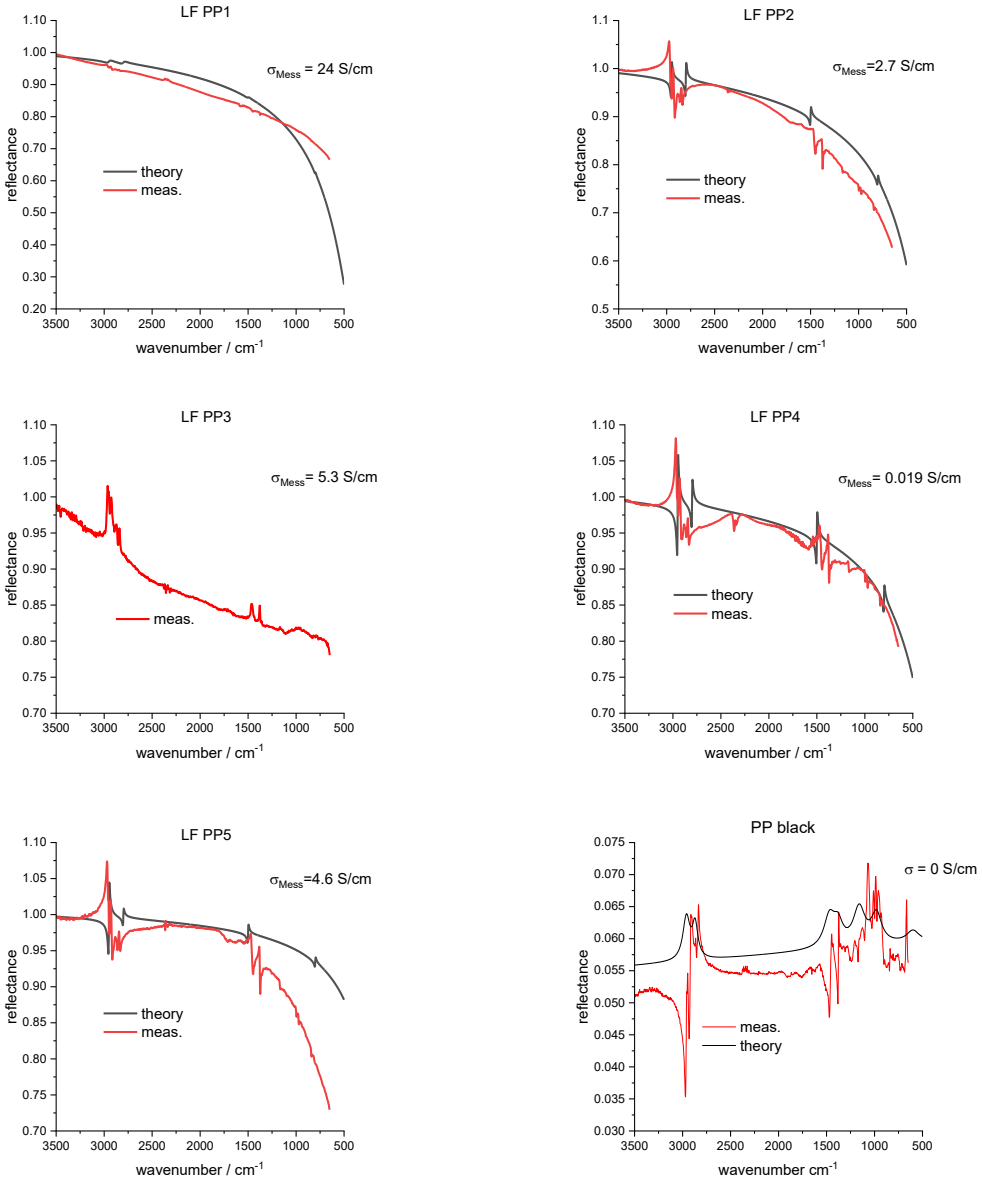

Figure 5. Comparison of measured (red) and modeled (black) IR reflectance spectra of different LF-PP samples (PP1–PP5) and black PP samples in the range 3500–500 cm^{-1}. The measured electrical conductivity σ_{mess} is indicated in the diagrams.

The present work does not aim at quantitative chemical analysis by FTIR, but at identifying fundamental physical limitations of infrared-based polymer identification.

The sample LF PP1 exhibited the highest specific electrical conductivity in the dataset at 24 S/cm. In its reflectance spectrum, virtually no pronounced peaks were observed. The curve appears flat and featureless over the entire mid-infrared range. This matches theoretical expectations for highly conductive polymers: the resonances of bound molecular vibrations are almost completely masked by free charge carriers. The simulated curve agrees well with the measurement, confirming the model's

validity in this regime. This sample illustrates the central finding of this study: as electrical conductivity increases, black polymer composites lose their characteristic IR signatures, making spectral identification practically impossible. Similar suppression of characteristic spectral features by free charge carriers has also been reported for electrically conductive inorganic material systems, where the optical response is dominated by free-electron contributions rather than localized vibrational or resonant excitations [23–25].

Sample LF PP2 shows a much lower conductivity of 2.7 S/cm. Accordingly, some residual vibrational peaks are still visible in the spectrum, although significantly attenuated. The fitted conductivity was 5 S/cm, which falls within an acceptable range considering possible measurement uncertainties and surface-related effects. The simulation successfully reproduces the spectral features and the increasing reflectance toward lower wavenumbers.

In the case of LF PP3 (measured conductivity 5.3 S/cm), no meaningful spectral fit was possible. The spectrum deviated substantially from the expected shape, and no consistent agreement with any model parameters could be achieved. Visual inspection revealed noticeable scratches and surface irregularities, most likely caused during sample processing or handling. These imperfections can lead to strong scattering and measurement artifacts. Consequently, this measurement is considered invalid, and no reliable conclusions can be drawn from it.

Sample LF PP4 had an unusually low measured conductivity of just 0.019 S/cm. In contrast, the spectrum could be fitted well with a conductivity value of 6.5 S/cm. This significant discrepancy strongly suggests that the conductivity measurement was likely faulty, possibly due to poor contact, localized inhomogeneities, or undetected contamination. The spectral fit, however, shows typical characteristics and good agreement with the measured curve. This case illustrates that spectral analysis can, under certain circumstances, provide a more reliable indication of bulk conductivity than four-point measurements, particularly when surface quality is suboptimal.

Sample LF PP5 occupies an intermediate position in the dataset. The measured conductivity was 4.6 S/cm, while the fitted value was 7 S/cm. The spectrum still shows partially recognizable vibrational features, albeit clearly damped. The fit is stable and matches the overall spectral shape. This sample demonstrates that in the range of moderate conductivity, meaningful spectral information remains accessible, and accurate modeling is still feasible.

The reference sample “PP black” exhibits zero electrical conductivity ($\sigma_{mess} = 0$ S/cm). In contrast to the conductive LF-PP samples, its infrared reflectance spectrum shows a clearly structured spectral shape with pronounced modulations and no decrease of reflectance toward lower wavenumbers. In particular, the reflectance remains nearly constant below approximately 1000 cm^{-1}, indicating the absence of a free-carrier-dominated response.

The measured spectrum can be adequately reproduced using a dielectric function composed solely of Lorentz oscillators, without inclusion of a Drude term. The fitted conductivity is $\sigma_{fit} = 0$ S/cm, fully consistent with the electrical measurement. The purpose of this fit is not a detailed reproduction of individual vibrational bands, but to demonstrate that the overall spectral shape—including the absence of low-wavenumber reflectance suppression—can be described without invoking free charge carriers. This result confirms that the low-frequency reflectance decay observed in conductive samples is a direct consequence of electrical conductivity rather than black coloration.

4. Conclusion

This study demonstrates that the applicability of FTIR spectroscopy for the identification of black polypropylene (PP) polymers is progressively limited by increasing electrical conductivity. The influence of free charge carriers on the infrared reflectance response becomes detectable already at very low conductivities on the order of $\sigma \approx 0.02$ S/cm, where a noticeable attenuation of characteristic vibrational features is observed. With further increased conductivity, the suppression of polymer-specific infrared bands becomes increasingly pronounced. The inclusion of a non-conductive black reference sample demonstrates explicitly that black coloration alone does not lead to suppression of infrared spectral features or to a decrease of reflectance at low wavenumbers. Only the presence of free charge carriers, i.e., finite electrical conductivity, gives rise to the Drude-like response observed in conductive polymer composites.

At conductivities exceeding approximately $\sigma \approx 20–25$ S/cm, no distinct vibrational modes of the polymer matrix can be identified anymore. In this regime, the infrared response is fully dominated by the free-electron contribution, resulting in a curved, featureless reflectance spectrum. Consequently, spectroscopic identification of the polymer using FTIR becomes fundamentally impossible.

This behavior, often attributed solely to black coloration, is shown to be primarily governed by electrical conductivity. The observed transition from vibration-dominated to free-carrier-dominated infrared response is consistent with recent studies on conductive carbon-based materials, where broadband, largely featureless optical absorption is governed by delocalized charge carriers rather than molecular vibrational modes [26]. In such systems, increasing electrical conductivity leads to a progressive suppression of spectroscopic signatures, independent of macroscopic coloration. This broader perspective confirms that the limitations of FTIR-based polymer identification identified in this work are of fundamental physical origin and extend beyond the specific polypropylene composites investigated here. Importantly, similar limitations can therefore also occur in non-black polymer materials that exhibit sufficiently high conductivity due to the incorporation of conductive fillers. These findings define a clear physical limitation of FTIR-based material identification in plastic recycling applications and underline the necessity of alternative analytical approaches for conductive polymer systems.

Alternative analytical methods must therefore be considered and implemented in sorting lines that handle significant fractions of electrically conductive plastic materials. One promising approach is laser-induced breakdown spectroscopy (LIBS), which has the potential to overcome the limitations of infrared-based methods by directly probing the elemental composition of the samples. LIBS offers high sensitivity and rapid data acquisition, making it, in principle, suitable for industrial process monitoring.

However, the applicability of LIBS as an in-line or on-line technique in plastic recycling environments has not yet been fully established. Challenges such as measurement stability, calibration robustness, and integration into existing sorting infrastructures require further systematic investigation. Consequently, additional experimental validation and process-oriented studies are necessary to assess the practical feasibility of LIBS for large-scale industrial deployment.

Use of AI tools declaration

The authors declare they have not used Artificial Intelligence (AI) tools in the creation of this article.

Acknowledgments

The authors acknowledge that all work presented in this study was conducted with the support of the Fraunhofer Institute for Chemical Technology (ICT).

Conflict of interest

The authors declare no conflicts of interest in this paper.

References

1. Plastics Europe, Plastics the fast facts 2024, accessed 7 October 2025. https://plasticseurope.org/knowledge-hub/plastics-the-fast-facts-2024/
2. Plastics Europe, The Circular Economy for Plastics—A European Analysis 2024. https://plasticseurope.org/knowledge-hub/the-circular-economy-for-plastics-a-european-analysis-2024/
3. Chen S, Hu YH (2024) Advancements and future directions in waste plastics recycling: From mechanical methods to innovative chemical processes. *Chem Eng J* 493: 152727. https://doi.org/10.1016/j.cej.2024.152727
4. Becker W (2006) Prozessanalytik in der Kunststoffindustrie. In: Kessler RW (ed) Prozessanalytik. Wiley, pp 551–570. https://doi.org/10.1002/3527608990.ch18
5. Irfan HB, Manasija B (2019) An IoT-based system for classification and identification of plastic waste using near infrared spectroscopy. In: Kundu S, Acharya US, De CK, Mukherjee S (eds) *Proceedings of the 2nd International Conference on Communication, Devices and Computing.* ICCDC 2019. Lecture Notes in Electrical Engineering, vol 602. Springer, Singapore. https://doi.org/10.1007/978-981-15-0829-5_65
6. Zhu S, Chen H, Wang M, et al. (2019) Plastic solid waste identification system based on near infrared spectroscopy in combination with support vector machine. *Adv Indust Eng Polymer Res* 2: 77–81. https://doi.org/10.1016/j.aiepr.2019.04.001
7. Pocheville A, Uria I, España P, Arnaiz S (2025) Raman spectroscopy integrated with machine learning techniques to improve industrial sorting of Waste Electric and Electronic Equipment (WEEE) plastics. *J Environ Manag* 373:123897. https://doi.org/10.1016/j.jenvman.2024.123897
8. Wan E, Tian D, Sun Z, Liu Y (2023) The online in situ detection of plastic and its combustion smoke via laser-induced breakdown spectroscopy. *Spectr Letters* 56: 62–72. https://doi.org/10.1080/00387010.2023.2165505
9. Abubaker SA, Chaqmaqchee FA, Taha AH (2021) Identification and characterization of different types of plastics wastes using X-ray diffraction and X-ray fluorescence techniques. *ARO* 9: 22–25. https://doi.org/10.14500/aro.10840

10. Becker W, Sachsenheimer K, Klemenz M (2017) Detection of black plastics in the Middle Infrared Spectrum (MIR) using photon up-conversion technique for polymer recycling purposes. *Polymers* 9: 435. https://doi.org/10.3390/polym9090435
11. Frederick W (1972) Optical Properties of Solids. Academic Press New York and London. https://doi.org/10.1016/C2013-0-07656-6
12. Fox M (2008) Optical properties of solids, Repr., with corr. Oxford master series in physics Condensed matter physics, vol. 3, Oxford University Press, Oxford. https://www.worldcat.org/isbn/9780199573370
13. Dressel M, Grüner G (2002) Electrodynamics of solids. Optical properties of electrons in matter. Cambridge University Press, Cambridge, New York, Melbourne. https://doi.org/10.1017/CBO9780511606168
14. Grosse P (1979) Freie Elektronen in Festkörpern. Hochschultext. Springer, Berlin, Heidelberg. https://doi.org/10.1007/978-3-642-95344-6
15. Youn SJ, Rho TH, Min BI, et al. (2007) Extended Drude model analysis of noble metals. *Phys Status Solid* 244: 1354–1362. https://doi.org/10.1002/pssb.200642097
16. Jung E, Lee S, Roh S, et al. (2014) Optical properties of graphite oxide and reduced graphite oxide. *J Phys D Appl Phys* 47: 265306. https://doi.org/10.1088/0022-3727/47/26/265306
17. Sutliff BP, Goyal S, Martin TB, et al. (2024) Correlating near-infrared spectra to bulk properties in polyolefins. *Macromolecules* 57: 2329–2338. https://doi.org/10.1021/acs.macromol.3c02290
18. Nan C-W, Shen Y, Ma J (2010) Physical properties of composites near percolation. *Annu Rev Mater Res* 40: 131–151. https://doi.org/10.1146/annurev-matsci-070909-104529
19. Choi H-J, Kim MS, Ahn D, Yeo SY, et al. (2019) Electrical percolation threshold of carbon black in a polymer matrix and its application to antistatic fibre. *Sci Rep* 9: 6338. https://doi.org/10.1038/s41598-019-42495-1
20. Ma PC, Siddiqui NA, Marom G, et al. (2010) Dispersion and functionalization of carbon nanotubes for polymer-based nanocomposites: A review. *Compos Part A Appl Sci Manufact* 41: 1345–1367. https://doi.org/10.1016/j.compositesa.2010.07.003
21. Schroder DK (2005) Semiconductor Material and Device Characterization. Wiley. http://onlinelibrary.wiley.com/book/10.1002/0471749095
22. Smits FM (1958) Measurement of sheet resistivities with the four-point probe. *Bell Syst Techn J* 37: 711–718. https://doi.org/10.1002/j.1538-7305.1958.tb03883.x
23. Guo R, Su F, Wang H, Guo Y, et al. (2019) Luminescence tuning of Layered Rare-earth Hydroxides (LRHs, R = Tb, Y) composites with 3-Hydroxy-2-naphthoic Acid and application to the fluorescent detection of Al3. *Inorg chem* 58: 4979–4988. https://doi.org/10.1021/acs.inorgchem.8b03636
24. Guo R, Li J, Chen L, Yu Z, et al. (2020) SDC/OS-LDH composite for highly sensitive fluorescence detection of Fe^{3+} at a much lower concentration. *Dalton Transact* 49: 10413–10420. https://doi.org/10.1039/d0dt01873b
25. Lu J, Zhang H, Li S, et al. (2020) Oxygen-vacancy-enhanced peroxidase-like activity of reduced Co_3O_4 nanocomposites for the colorimetric detection of H_2O_2 and Glucose. *Inorg Chem* 59: 3152–3159. https://doi.org/10.1021/acs.inorgchem.9b03512
26. Sun Z, Liao Y, Zhang Y, et al. (2025) Sustainable carbon materials in environmental and energy

applications. *Sustain Carbon Mater* 1: e007. https://doi.org/10.48130/scm-0025-0002